Phase diagrams and morphological evolution in wrapping of rod-shaped elastic nanoparticles by cell membrane: A two-dimensional study

Xin Yi and Huajian Gao*
School of Engineering, Brown University, Providence, Rhode Island 02912, USA
(Received 17 February 2014; published 24 June 2014)

A fundamental understanding of cell-nanomaterial interaction is essential for biomedical diagnostics, therapeutics, and nanotoxicity. Here, we perform a theoretical analysis to investigate the phase diagram and morphological evolution of an elastic rod-shaped nanoparticle wrapped by a lipid membrane in two dimensions. We show that there exist five possible wrapping phases based on the stability of full wrapping, partial wrapping, and no wrapping states. The wrapping phases depend on the shape and size of the particle, adhesion energy, membrane tension, and bending rigidity ratio between the particle and membrane. While symmetric morphologies are observed in the early and late stages of wrapping, in between a soft rod-shaped nanoparticle undergoes a dramatic symmetry breaking morphological change while stiff and rigid nanoparticles experience a sharp reorientation. These results are of interest to the study of a range of phenomena including viral budding, exocytosis, as well as endocytosis or phagocytosis of elastic particles into cells.

DOI: 10.1103/PhysRevE.89.062712 PACS number(s): 87.16.D−, 46.70.Hg, 87.17.Aa, 87.17.Rt

I. INTRODUCTION

Understanding the cellular uptake of nanoparticles is essential to a wide range of applications concerning biomedical diagnosis, therapy, and drug delivery. During the past decade, substantial research progress has been achieved on the effect of size [1–3], shape [3–16], and surface structure [17–19] of nanoparticles on their cellular uptake. In addition, there has also been increasing interest in cell interaction with elastic nanoparticles. For example, it has been shown that phagocytosis of soft microparticles can be hindered by particle deformation [20]. Recent theoretical study indicates that soft nanoparticles require stronger adhesion energy to be completely engulfed than stiff nanoparticles [21], which may have important biological implications on the cell entry mechanism of HIV. Nanoparticles decorated with stiffer ligands are more easily engulfed than those coated with softer ligands [18]. Moreover, elasticity can strongly influence the flow behavior of cells. For example, sickle red blood cells of different morphologies and membrane rigidities exhibit different flow efficiency in shear flow [22–24].

Most existing theoretical work on the interaction between nanoparticles and cells has focused on symmetric or axisymmetric geometries [21,25–28]. Although some theoretical studies have accounted for asymmetric deformation of a membrane as it wraps around a single rigid rod-shaped nanoparticle or multiple spherical nanoparticles [8–11,29–31], so far no theoretical investigations have been performed for cell membrane wrapping around rod-shaped elastic nanoparticles where both the nanoparticle and membrane can undergo asymmetric deformation.

Here we perform a theoretical study on the adhesive wrapping of an elastic rod-shaped nanoparticle by a lipid membrane with asymmetric deformation. We investigate how the wrapping degree and morphologies of the nanoparticle and membrane depend on the nanoparticle size and shape, adhesion energy, membrane tension, and bending rigidity ratio between the particle and membrane. We determine the wrapping phase diagram for cellular uptake of a class of two-dimensional (2D) elastic nanoparticles that can be modeled as vesicles, probing the transitions between full wrapping, partial wrapping, and no wrapping states, as well as the particle orientation phase diagram for the interaction of a short and stiff rod-shaped nanoparticle with membrane. Although our analysis is limited to two dimensions, some results are generic and can be safely extrapolated to three-dimensional cases. We also discuss possible implications of our results on relevant biological processes such as viral budding and endocytosis.

II. MODEL AND METHODS

While we note that an elastic nanoparticle can be modeled in a number of alternative ways, here we limit our attention to a class of elastic nanoparticles that can be modeled as a 2D vesicle with constant contour length L_t and fixed area A. For such a 2D elastic nanoparticle wrapped by an initially flat cell membrane with elastic deformation in both the particle and membrane, as shown in Fig. 1(a), the total energy of the system per unit length in the out-of-plane direction can be described by the Canham-Helfrich functional as [21,25,28,32–35]

$$E_{\text{tot}} = \sum_{i=1,2,3} \int \frac{\kappa_i}{2} \dot{\psi}_i^2 ds_i + PA + \sigma \Delta l - \gamma l_3, \qquad (1)$$

where P is a Lagrange multiplier enforcing the enclosed area A of the nanoparticle; γ is the specific adhesion energy, and l_3 is the length of the contact region; σ is the membrane tension, which is conjugated to the excess length $\Delta l = \sum_{i=2,3} \int (1 - \cos\psi_i) ds_i$ induced by wrapping; ψ_i, s_i, and κ_i $(i = 1,2,3)$ are the tangent angles, arclength, and bending stiffness of the three regions, respectively [see Fig. 1(a)]. The superposed dot in the first term in Eq. (1) denotes derivative with respect to the arclength s, and subscripts 1, 2, and 3 are used to identify quantities associated with the inner free, outer free, and wrapped regions, respectively. Since $\int_0^{l_3} \dot{\psi}_3 ds_3 - \int_0^{l_1} \dot{\psi}_1 ds_1 = 2\pi$ and the circumference L_t of the nanoparticle is fixed, a spontaneous or intrinsic curvature c_0 associated with the elastic

*huajian_gao@brown.edu

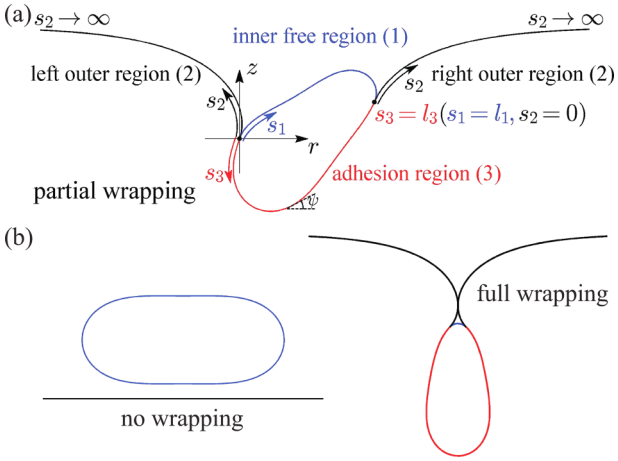

FIG. 1. (Color online) Schematic of a soft elastic particle modeled as a vesicle and wrapped by an initially flat membrane in the adopted two-dimensional Cartesian coordinate rz. (a) The geometry of the system with tangent angle ψ. Arclengths s_i ($i = 1,2,3$) are defined along the particle and the outer free part of the membrane; s_1, s_2 of the left outer region, and s_3 are measured from the left contact edge, and s_2 of the right outer region is measured from the right contact edge $s_2 = 0$ ($s_1 = l_1$, $s_3 = l_3$). (b) Schematic for the states of no wrapping with zero contact length and full wrapping in which the left and right sides of the membrane touch each other on the top of the particle. Partial wrapping corresponds to the intermediate scenario with incomplete wrapping as shown in (a).

nanoparticle would only result in an extra constant energy term in $E_{\rm tot}$ in Eq. (1) [34,35] and therefore needs not be explicitly considered. While recognizing important exceptions such as the possible formation of clathrin or caveolin coats during the wrapping process, for simplicity we assume $\kappa_3 = \kappa_1 + \kappa_2$ throughout the analysis. All lengths are scaled by the effective radius of the particle, $a = L_t/(2\pi)$, and the area of the nanoparticle is reduced as $v = A/(\pi a^2) \leqslant 1$. As v gradually increases, the shape of such a free-standing particle evolves from a concave dumbbell to a short rod and eventually to a circle at $v = 1$. Hereinafter both the concave dumbbell and short rod shapes are referred to as rodlike shapes. Other dimensionless parameters are

$$\bar{\sigma} \equiv 2\sigma a^2/\kappa_2 \quad \text{and} \quad \bar{\gamma} \equiv 2\gamma a^2/\kappa_2.$$

Since the bending energy of a planar elastica has the same form as the first term in Eq. (1), our analysis also applies to the wrapping of a two-dimensional inextensible elastic thin shell capsule by a lipid membrane.

An isolated particle with a prescribed reduced area $v < 1$ has a rodlike shape. Such a particle with area constraint would exhibit asymmetric deformation during the wrapping process. Here we employ a numerical optimization technique to determine the minimum energy state at each given wrapping degree $f = l_3/L_t$ defined as the ratio between the length of the contact region and the circumference of the nanoparticle. With geometric relations $\dot{r} = \cos\psi$ and $\dot{z} = \sin\psi$, the elastic deformation energy $E_{\rm el} = E_{\rm tot} + \gamma l_3$ in the region i ($i = 1,2,3$) at a given wrapping degree f can be represented as a function of the unknown tangent angle $\psi_i(s_i)$ which is approximated by a Fourier series as [26,27,36]

$$\psi_i(s_i) = \psi_0^{(i)} + \left(\psi_l^{(i)} - \psi_0^{(i)}\right)\frac{s_i}{l_i} + \sum_{j=1}^{N} a_j^{(i)} \sin\frac{\pi j s_i}{l_i}. \quad (2)$$

Here N is the number of Fourier modes, which is chosen as $N = 80$ in our calculations; $a_j^{(i)}$ are the Fourier amplitudes, s_i is the arclength, and l_i is the length of the considered region i ($i = 1,2,3$); and $\psi_0^{(i)}$ and $\psi_l^{(i)}$ are the tangent angles at $s_i = 0, l_i$, respectively. For a given wrapping degree f, it can be easily seen that $l_1 = 2(1-f)\pi$ and $l_3 = 2f\pi$. To approximate the condition $s_2 \to \infty$, the length l_2 of the outer membrane region can be treated as either a certain large number or an unknown parameter determined by a prescribed length of the membrane projection. Our calculations indicate that the choice of these conditions will not affect the final results. For the latter, we set the length of the outer free membrane projection on each side to be $20a$.

The boundary and constraint conditions provide either input parameters or equality constraints during energy minimization. At $s_2 \to \infty$, the outer free membrane becomes asymptotically flat which requires $\psi_l^{(2)} = 0$. Since we adopt the coordinate with origin at the left contact edge, the continuity of the coordinate (r,z) for the three regions at the origin is satisfied automatically. The continuity of the coordinate (r,z) at the right contact edge, the continuity of the tangent angles ψ at both left and right contact edges, and the prescribed reduced area v are enforced as equality constraints. The elastic energy as a function of $\psi_i(s_i)$ under these constraints at a given f is minimized with respect to the Fourier amplitudes a_j, tangent angles ψ_0 and ψ_l at both contact edges, and l_2 for both outer free regions using sequential quadratic programming [37]. Once the tangent angles ψ given by Eq. (2) are known, the elastic energy and corresponding shapes (of the particle and membrane) can be determined.

III. RESULTS

Figures 2(a)–2(c) show the elastic energy change $\Delta E_{\rm el} = E_{\rm el} - E_{\rm el}^0$ as a function of the wrapping degree f, where $E_{\rm el}^0$ is the reference energy before the nanoparticle contacts the membrane. The open triangle on each curve corresponds to full wrapping. The bold (red) solid segments on some curves in Figs. 2(a) and 2(b) indicate the occurrence of asymmetric deformation as the wrapping degree f reaches a critical value f_c slightly larger than 0.5. At $f < f_c$, a soft particle (e.g., $\kappa_1/\kappa_2 = 0.1$) would contact with the membrane with its flattened side, while a relatively stiff (e.g., $\kappa_1/\kappa_2 = 1$) or rigid ($\kappa_1/\kappa_2 \to \infty$) rodlike particle would align its long axis parallel to the membrane [see Figs. 2(d) and 2(e)]. As the wrapping proceeds, the particle and membrane undergo a transition from a symmetric configuration at $f < f_c$ to an asymmetric one, followed by another symmetric configuration in the late stage. Compared to the initial symmetric morphology of particles with long axis parallel to the membrane at $f < f_c$, a soft particle would undergo a dramatic symmetry breaking transition while a stiff particle would reorient itself sharply so that its long axes are realigned perpendicular to the membrane in the second symmetric morphology associated with the late stage of wrapping [Figs. 2(d) and 2(e)]. The adoption of an

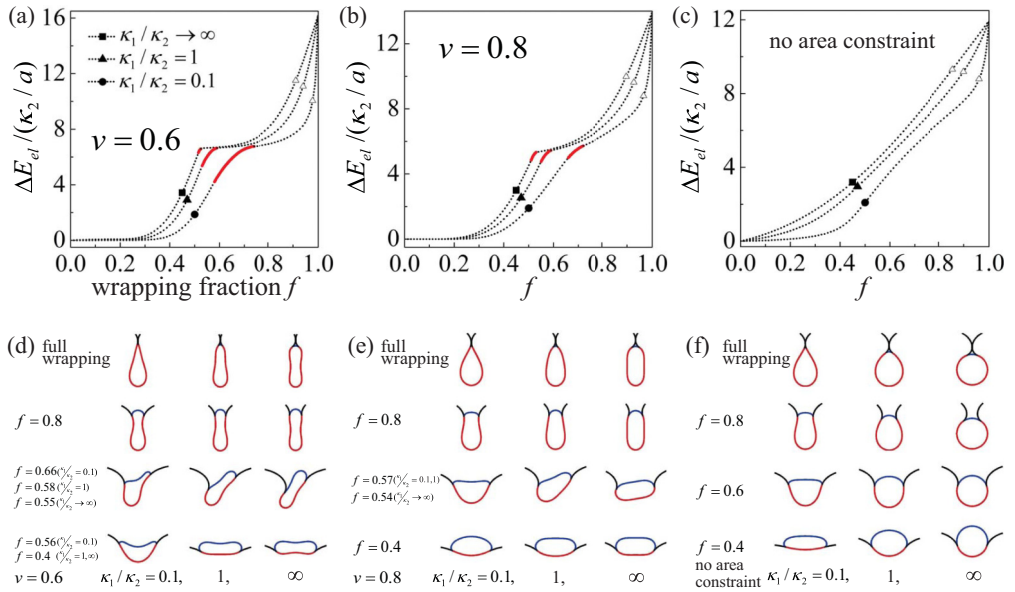

FIG. 2. (Color online) (a–c) Elastic energy $\Delta E_{\rm el}$ as a membrane wraps around a nanoparticle with wrapping degree f for different reduced areas v and κ_1/κ_2 at $\bar{\sigma} = 1$. The open triangle on each curve corresponds to full wrapping. The bold (red) solid regions on some curves indicate asymmetric deformation. (d–f) Selective wrapping configurations at $\bar{\sigma} = 2$ for different enclosed areas and particle-membrane rigidity ratios κ_1/κ_2.

asymmetric morphology results from a significant decrease in the total elastic energy due to symmetry breaking. It is found that $f_c - 0.5$ is inversely proportional to the rigidity ratio κ_1/κ_2. In general, smaller bending rigidity ratio κ_1/κ_2, which gives rise to a more flattened particle with smaller excess length Δl and smaller membrane tension energy $\sigma\Delta l$, and larger membrane tension lead to larger asymmetric regions [see Figs. 2(a) and 2(b), Fig. S1(a) [38], and Figs. S1(b) and S1(c) [38] at $\kappa_1/\kappa_2 = 1,5,\infty$]. A few exceptional examples with no symmetry breaking are observed for very soft particles ($\kappa_1/\kappa_2 = 0.1$) with $v = 0.8$ at $\bar{\sigma} = 2$ in Fig. S1(b) and with $v = 0.95$ [Figs. S1(c) and S2] in the Supplemental Material [38], which can be attributed to the fact that there is no longer an energy drop from symmetric to asymmetric morphologies for very soft particles. It is also observed that the value of f at full wrapping increases as the rigidity ratio κ_1/κ_2 decreases and membrane tension $\bar{\sigma}$ increases [38]. Note that in our previous study [21] only the symmetric configuration was observed since the enclosed area was not prescribed during the wrapping process [Figs. 2(c) and 2(f)].

A free-standing 2D elastic nanoparticle with a small reduced area (e.g., $v = 0.6$) exhibits a concave shape as shown in Fig. 2(d) for $\kappa_1/\kappa_2 \to \infty$. Such a concave shape would lead to a narrow gap between the adhered particle and membrane at initial contact (Fig. 3). The size of the gap decreases as the wrapping degree f increases and a full contact is achieved when f exceeds about 0.1. The existence of a narrow gap was also observed between a round particle adhering to an oblate vesicle [39]. Here the adhesive interaction between the nanoparticle and membrane is characterized by a contact potential with vanishing interaction range as given in Eq. (1). Based on a recent study showing that the size of the interaction range plays an important role in the wrapping process [40], the gap size is expected to depend on the interaction range.

The total energy difference $\Delta E = E_{\rm tot} - E^0_{\rm el}$ corresponds to the sum of the elastic energy difference $\Delta E_{\rm el}$ and adhesion energy $-f\gamma L_t$. Figure 4 shows $\Delta E(f)$ as a function of the wrapping degree f for different $\bar{\gamma}$ in the case $v = 0.95$, $\kappa_1/\kappa_2 = 0.1$, and $\bar{\sigma} = 0.1$. The behavior of $\Delta E(f)$ indicates that there exist five possible phases when $\bar{\sigma}$ is very small (Fig. 4). For relatively small adhesion energy $\bar{\gamma}$, ΔE increases monotonically with f and no wrapping is possible. As $\bar{\gamma}$ increases, the stable state changes from no wrapping to partial wrapping. Further rise in $\bar{\gamma}$ results in a global minimum at a state of partial wrapping and an energy barrier to reach the (metastable) state of full wrapping. With $\bar{\gamma}$ continuously rising, the stable state of partial wrapping becomes metastable while full wrapping becomes stable. In the regimes of two coexisting states of partial and full wrapping, the one with lower energy is underlined (Fig. 4). If $\bar{\gamma}$ is large enough, the energy barrier to full wrapping vanishes and full wrapping becomes the

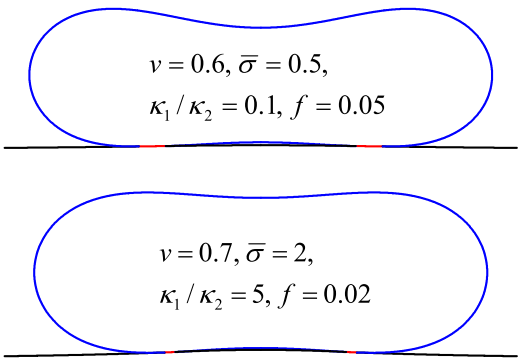

FIG. 3. (Color online) A narrow gap exists at the initial contact between a flat membrane and an elastic particle with small reduced area v.

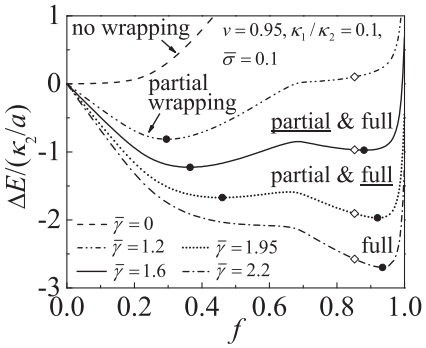

FIG. 4. Total energy change ΔE of five possible wrapping states as a function of the wrapping degree f for different $\bar{\gamma}$ with $v = 0.95$, $\kappa_1/\kappa_2 = 0.1$, and $\bar{\sigma} = 0.1$. The solid circles on curves correspond to the local minima. The open squares correspond to full wrapping. The underlined wrapping state has energy lower than its coexisting wrapping state.

only stable state. For each phase, there exists a stable (global energy minimum) state and possibly a metastable (local energy minimum) state. When $\bar{\sigma}$ is sufficiently large, there are no longer coexisting states of partial and full wrapping, and the stable state simply changes from no wrapping to partial wrapping then to full wrapping as $\bar{\gamma}$ increases. Note that the solutions at solid circles are unphysical in cases when full wrapping (marked by the open squares) arises before f reaches the position marked by the solid circles. In these cases, full wrapping occurs as the membrane comes in contact above the nanoparticle and is not necessarily the state of zero slope along the energy profile.

With the knowledge of energy functions at different values of κ_1/κ_2, v, $\bar{\sigma}$, and $\bar{\gamma}$, the phase diagrams of wrapping are determined and shown in Figs. 5 and S3 [38]. Note that the solution at $f = 1$ is usually unphysical because in that case the two opposing parts of the membrane will have met and crossed each other above the nanoparticle. Therefore, the state of full wrapping needs to be carefully defined [Fig. 1(b)]. At the late stage of wrapping, both particle and membrane display symmetric morphologies, and the shape equation for the outer free part of the membrane associated with a given wrapping angle $\psi_0^{(2)}$ has the analytical solution $\psi_2 = 4\arctan[\tan(\psi_0^{(2)}/4)\exp(-s_2\sqrt{\bar{\sigma}/2})]$, where s_2 is the rescaled arclength of the outer free part [41]. With the relations $\dot{r} = \cos\psi$ and $\dot{z} = \sin\psi$, the $r(s_2)$ and $z(s_2)$ coordinates can be determined as [21]

$$r(s_2) = r_0 + s_2 - \sqrt{\frac{2}{\bar{\sigma}}}\frac{1-\cos\psi_0^{(2)}}{\coth(\sqrt{\bar{\sigma}/2}s_2) + \cos\frac{\psi_0^{(2)}}{2}},$$

$$z(s_2) = z_0 + \sqrt{\frac{8}{\bar{\sigma}}}\sin\frac{\psi_0^{(2)}}{2}\left[1 - \frac{\operatorname{csch}(\sqrt{\bar{\sigma}/2}s_2)}{\coth\left(\sqrt{\frac{\bar{\sigma}}{2}}s_2\right) + \cos\frac{\psi_0^{(2)}}{2}}\right],$$

where r_0 and z_0 are the coordinates of the contact edge and $\psi_0^{(2)}$ is the tangent angle at $r = r_0$. For a given set of values for r_0, $\psi_0^{(2)}$, and $\bar{\sigma}$, the minimum of $r(s_2)$ for the right outer free membrane and the maximum of $r(s_2)$ for the left outer free membrane can be determined. The full wrapping condition is then found from the condition that these extreme values are equal, corresponding to the situation when the two opposing parts of the membrane come into contact, as shown in Fig. 5. The critical condition for a rigid circular particle to be fully wrapped by a membrane is then [42]

$$\sqrt{\frac{\bar{\sigma}}{2}}\sin\psi_0^{(2)} = \sqrt{2} - 2\cos\frac{\psi_0^{(2)}}{2} + \ln\left(\tan\frac{\pi}{8}\cot\frac{\psi_0^{(2)}}{4}\right),$$

with the contact angle $\psi_0^{(2)} = \arccos[1-(1-\sqrt{\bar{\gamma}})^2/\bar{\sigma}]$.

It may be interesting to compare the wrapping phase diagram for particles without area constraints calculated in our previous study [21] with those under reduced area constraints [Figs. 5(a)–5(c)]. First, for a membrane wrapping around a rigid circular particle, the total energy evolves as

$$\frac{\Delta E}{\kappa_2/a} = 8\sqrt{2\bar{\sigma}}\sin^2\frac{f\pi}{4} + f\pi + \bar{\sigma}\,[f\pi - \sin(f\pi)] - f\pi\bar{\gamma}.$$

The condition $\partial\Delta E/\partial f|_{f=0} = 0$ gives the minimum adhesion energy necessary for partial wrapping as $\bar{\gamma}_{\min} = 1$ [42]. For such a particle, $\partial^2\Delta E/\partial f^2 = 0$ gives $f = 1$, which means that the only inflection point of the energy profile is at $f = 1$, and that there is no energy barrier for ΔE for any $\bar{\gamma}$ as f varies and therefore no coexistence of partial and full wrapping states in membrane wrapping of a rigid circular particle regardless of the value of membrane tension $\bar{\sigma}$. For

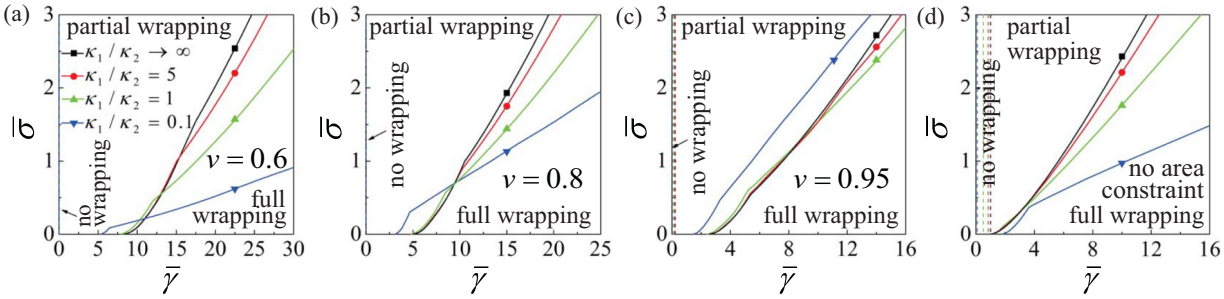

FIG. 5. (Color online) Wrapping phase diagrams with respect to normalized adhesion energy $\bar{\gamma}$ and membrane tension $\bar{\sigma}$ at different rigidity ratios κ_1/κ_2 and reduced areas v. (a–c) Cases with reduced areas $v = 0.6$, 0.8, and 0.95. (d) The case investigated in our previous study [21] with no area constraint is provided here for comparison with cases (a)–(c). Dashed lines indicate boundaries between no wrapping and partial wrapping states. Solid lines indicate boundaries between partial and full wrapping states. In cases (a) and (b), the adhesion energy for partial wrapping is so small that the dashed lines almost overlap with the $\bar{\sigma}$ axis.

elastic particles without area constraints, $\bar{\gamma}_{\min}$ decreases as κ_1/κ_2 decreases, as the easily flattened softer particles lead to smaller elastic energy; however, $\bar{\gamma}$ needs to increase to attain full wrapping. When $\bar{\sigma} \leqslant 0.5$, there are small differences between the transition lines from the state of partial wrapping to full wrapping for different κ_1/κ_2. As $\bar{\sigma}$ increases further, the differences become large and strikingly sensitive to κ_1/κ_2 [see Fig. 5(d)]. This phenomenon can also be understood by comparing the maximum slopes of the elastic energy profiles at different κ_1/κ_2 (Figs. 2 and S1), since the condition for full wrapping to be the only stable state requires $\Delta E(f)$ to be a monotonically decreasing function or $\bar{\gamma}$ larger than the maximum slope of the elastic energy profile before f reaches the critical value for full wrapping indicated by the open symbols in Figs. 2 and S1. A similar effect of elasticity on the wrapping states is also observed for particles with constrained areas, as shown in Figs. 5(a)–5(c). For noncircular rod-shaped particles (e.g., those with $v = 0.6$, 0.8, and 0.95), $\bar{\gamma}_{\min}$ is significantly smaller than 1 since the initial wrapping causes less bending deformation. Compared to Fig. 5(d), a significant difference in Figs. 5(a)–5(c) is that, as $\bar{\sigma}$ is smaller than a certain value, softer particles may require smaller $\bar{\gamma}$ to attain full wrapping. For example, for $\bar{\sigma} = 0.5$ and $v = 0.8$ shown in Fig. 5(b), particles with bending rigidity $\kappa_1 = \kappa_2$ require smaller $\bar{\gamma}$ than stiffer ones to attain full wrapping and particles with $\kappa_1 = 0.1\kappa_2$ require even smaller $\bar{\gamma}$ than those with $\kappa_1 = \kappa_2$. This phenomenon is reflected in the elastic energy profile at $\bar{\sigma} = 0.5$ in Fig. S1(b) where stiffer particles exhibit larger maxima of energy slopes [38], indicating that higher $\bar{\gamma}$ would be required for full wrapping. As the reduced area v increases, the phase diagram becomes more complex. In the case of $v = 0.95$, particles with $\kappa_1 = 0.1\kappa_2$ require smaller $\bar{\gamma}$ than all the stiffer ones to attain full wrapping for the calculated range of $\bar{\sigma} \leqslant 3$; when $\bar{\sigma} \leqslant 1.5$, there are very small differences between the transition lines from the state of partial wrapping to full wrapping for $\kappa_1/\kappa_2 = 1$, 5, and ∞. The difference becomes larger as $\bar{\sigma}$ increases. The kinks on the phase boundaries in regions of relatively small $\bar{\sigma}$ indicate coexistence of partial and full wrapping states whose detailed phase diagrams are shown in Fig. S3 [38]. For particles with a prescribed reduced area v, the coexistence region exists only under sufficiently small $\bar{\sigma}$, with size increasing as the rigidity ratio κ_1/κ_2 increases [see Figs. S3(a)–S3(c)]. In contrast, for particles without area constraints, the coexistence region exists also under sufficiently small $\bar{\sigma}$, but its size decreases as the rigidity ratio κ_1/κ_2 increases, as shown in Fig. S3(d) [38]. A comparison of Figs. 5(a)–5(d) shows that the wrapping phase diagrams strongly depend on the value of the reduced area v, especially when v is close to 1. This is presented in Fig. S4 with further details [38].

Rigid particles with different reduced areas v exhibit different shapes. The shape effects of rigid 2D particles on cellular uptake can be extracted from Fig. 5 for different values of the constrained area v. When this is done, the results are compared together in Fig. 6. The $\bar{\gamma}$ required for full wrapping decreases as v increases. In other words, thinner and longer 2D rigid particles with larger aspect ratios require larger adhesion energy $\bar{\gamma}$ than thicker and shorter ones with smaller aspect ratios to attain full wrapping or, simply, slender particles are more resistant to full wrapping. This behavior

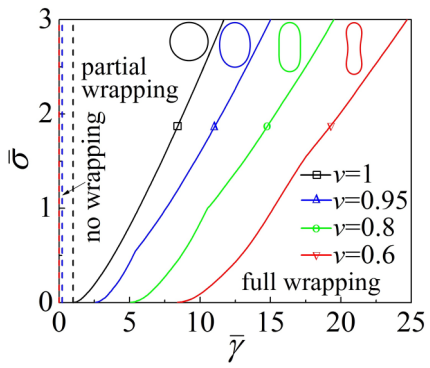

FIG. 6. (Color online) Wrapping phase diagram with respect to normalized adhesion energy $\bar{\gamma}$ and membrane tension $\bar{\sigma}$ for rigid particles with the same circumference but different enclosed areas. Shapes from left to right correspond to $v = 1$, 0.95, 0.8, and 0.6, respectively.

is a direct consequence of the energy profile in Fig. 2 where the black dotted curve corresponding to smaller v is seen to have larger slope. Particles with different v (shapes) in Fig. 6 have the same circumference L_t but different areas A. For particles with the same area A but different circumferences L_t (Fig. S5), the effective radius is redefined as $a = \sqrt{A/\pi}$ instead of $a = L_t/(2\pi)$. It can be shown that the corresponding phase diagram can be obtained from Fig. 6 through a linear scaling mapping $(v\bar{\gamma}, v\bar{\sigma}) \rightarrow (\bar{\gamma}, \bar{\sigma})$. For example, the point with coordinate (15.34,2) on the green curve ($v = 0.8$) in Fig. 6 is mapped to the point with coordinate $(15.34 \times 0.8, 2 \times 0.8) = (12.272, 1.6)$ on the green curve ($v = 0.8$) in Fig. S5 [38]. A comparison of Figs. 6 and S5 indicates that the shape effect is less striking for particles with the same area than with the same circumference. This property should also be valid for soft particles since the linear scaling mapping only depends on v rather than κ_1/κ_2.

Another interesting phenomenon is the sudden orientational change of rigid or relatively stiff and short rod-shaped nanoparticles around the wrapping degree of $f = 0.5$, as indicated in Fig. 2. In the early stage of wrapping, the rod-shaped nanoparticles align their long axes parallel to the membrane and remain in that configuration until the critical point of reorientation is reached, at which the nanoparticles suddenly realign their long axes perpendicular to the membrane and remain in this configuration during the late stage of wrapping. Since the slopes of the elastic energy profile $\Delta E_{\rm el}$ have similar values at reorientation and at full wrapping, the orientation phase diagram describing transition boundaries between different nanoparticle orientations (Fig. 7) is similar to the wrapping phase diagram describing different wrapping states (Fig. 6). As v decreases, $\bar{\gamma}$ needs to increase in order to maintain the perpendicular configuration. In Fig. 7 we have excluded the cases with coexisting parallel and perpendicular configurations, and only consider situations in which the total energy difference $\Delta E(f) = \Delta E_{\rm el}(f) - \gamma f L_t$ is a monotonically decreasing function when the nanoparticles adopt the perpendicular configuration relative to the membrane. The orientation phase diagram for the situation that particles have the same area A but different circumferences L_t can also be simply obtained from Fig. 7 through the same linear scaling

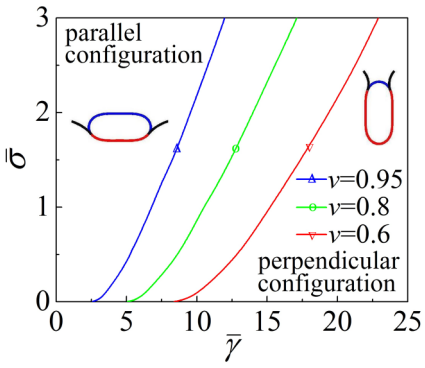

FIG. 7. (Color online) Particle orientation phase diagram with respect to normalized adhesion energy $\bar{\gamma}$ and membrane tension $\bar{\sigma}$ for rigid rod-shaped nanoparticles with the same circumference but different enclosed areas. The insets show parallel and perpendicular configurations in the case of $v = 0.8$.

mapping $(v\bar{\gamma}, v\bar{\sigma}) \rightarrow (\bar{\gamma}, \bar{\sigma})$ used in the preceding analysis for Fig. 6.

IV. DISCUSSION

Figure 2 shows that very soft particles ($\kappa_1/\kappa_2 = 0.1$) with a relatively small reduced area ($v = 0.6$ and 0.8) exhibit a dramatic morphological change from a symmetric parachute-like shape to an asymmetric slipperlike shape in the midstage of membrane wrapping as the reduced area v decreases. An interesting phenomenon is that red blood cells moving in a shear flow adopt similar complex morphologies [22,43]. Numerical studies show that a moving vesicle with the bending rigidity of a healthy red blood cell exhibits a symmetric parachutelike shape at the condition of a large reduced area v or a large flow velocity. Once v is below a critical value around 0.7, the symmetric parachutelike shape develops instability and the cell transforms into an asymmetric slipperlike shape no matter how large the flow velocity is [22]. Further numerical analysis shows that membrane bending rigidity also has a dramatic effect on the morphological change of red blood cells with a low reduced area (e.g., $v = 0.6$). Lower stiffness leads to an asymmetric slipperlike shape and larger stiffness results in a pearlike shape with slight asymmetry [22]. These observations are mysteriously similar to those found in the present wrapping problem [see the third row from the top in Fig. 2(d)]. Such v- and rigidity-dependent features shared by these two physically different phenomena are suggesting that there may be deep connections between the deformation shape, area constraint, bending stiffness, and types of loading on the behaviors of elastic particles.

Although the present study is restricted to two dimensions, some conclusions are generic and can be safely extrapolated to three dimensions. For example, 2D short rigid anisotropic nanoparticles or elastic nanoparticles with a prescribed reduced area undergo a dramatic morphological change induced by the membrane wrapping, and there exists an asymmetric shape transition in the midstage of wrapping. This phenomenon is mainly due to the high bending energy cost at the highly curved regions of rod-shaped nanoparticles and should be generic for both 2D and three-dimensional (3D) cases. Theoretical results [8–10] and molecular dynamics simulations [13–15] have shown that 3D rigid ellipsoidal, rod-shaped, and even hemisphere-shaped particles experience an orientational change in the midstage of wrapping. Another consequence of this high energy cost associated with bending around highly curved tips is that longer and thinner rigid rods with tips of higher curvature require larger adhesive energy than broader, shorter, and rounder ones with the same circumference but different enclosed areas or the same enclosed area but different circumferences to attain full wrapping (see Figs. 6 and S5). Similar phenomena have been found in numerical simulations and experiments for 3D rodlike nanoparticles under the constraint of the same area but different volume [10] or the same volume but different area [5,10]. Asymmetric morphology could appear when a 3D elastic nanoparticle with a prescribed reduced volume (defined as the ratio of the enclosed volume over the volume of a sphere having the same surface area) and anisotropic shape is wrapped by a cell membrane. Similar to the 2D case shown in Fig. 2(f), only the axisymmetric configuration was considered for 3D soft particles in Ref. [21].

The orientational change of short rod-shaped nanoparticles indicates that, no matter what the initial position or orientation such a particle take, a complete membrane wrapping or nanoparticle budding always ends up with a configuration with the rod-shaped nanoparticle aligning its long axis perpendicular to the cell membrane. Such reorientation of short nanoparticles seems ubiquitous in the budding and endocytosis of virus [44–46], and the orientation combined with membrane deformation provides information on the stage of budding process and endocytosis. For example, short rod-shaped fowlpox and pigeonpox viruses align their long axes parallel to the membrane of infected chick embryo fibroblasts in the initial stage and midstage of budding but eventually bud out of the cells with their long axes perpendicular to the membrane [44]. Similar phenomena are observed during the cell entry of vesicular stomatitis viruses by endocytosis [45]. Recent numerical simulations have shown that two adsorbed nanoparticles form a short linear cluster on the membrane surface of a vesicle at a large reduced volume but induce a short membrane tube on a vesicle at a small reduced volume [31]. This is consistent with our result in Fig. 7 in view of the fact that the conjugated membrane tension is greater at a larger reduced volume, though the cooperative wrapping of particles strongly depends on the range of interaction potential between particles and membrane [40]. Based on similar geometries and induced wrapping configurations, the particle-chain-induced short linear aggregation of nanoparticles adhering on the surface and short membrane tubulation can be considered as examples analogous to the parallel configuration at large membrane tensions in the early stage of wrapping and perpendicular configuration at small membrane tensions in the late stage of wrapping, respectively.

As Figs. 6 and S5 indicate, 2D rigid rod-shaped nanoparticles or particles with relatively small reduced areas (e.g., $v = 0.6$) require larger adhesive energy $\bar{\gamma}$ to attain full wrapping than round particles or particles with larger reduced areas. This shape-dependent uptake of short nanoparticles has important implications on the design of efficient endocytosis and drug or gene delivery systems. It has been observed

experimentally that ellipsoidal nanoparticles have a lower cellular uptake rate [3–6]. For example, the rate of cellular uptake of round particles is greater than that of rod-shaped particles with aspect ratio of 1:3, which in turn is greater than that of nanoparticles with even higher aspect ratio of 1:5 [3]. This is consistent with our theoretical results in Figs. 5, 6, and S5. Taking advantage of the shape effects on cellular uptake, nanoparticles can be designed to be cylindrical or elliptical to extend their circulation time in blood [6,47], or their labeling and tracking time as biomarkers on cell membranes [9]. Elastic rod-shaped nanoparticles can further amplify the shape effect (see Fig. 5). Through precise control of the reduced area of 2D elastic nanoparticles or the reduced volume of 3D elastic nanoparticles, the shape of these soft particles can be adjusted. Such elastic nanoparticles with tunable shapes may be used to design smart drug delivery systems. For example, researchers can design elongated drug nanoparticles (by controlling their enclosed volume in three dimensions) when the nanoparticles are in the circulation system and expand the particle to a rounder shape (by increasing the enclosed volume) to facilitate membrane wrapping as the particles reach their target cells. For nanoparticles coated with ligands, the adhesion energy $\gamma = \xi_L e_{RL}$ depends on the ligand density ξ_L and the energy of a single receptor-ligand bond e_{RL}. Taking typical parameter values as $\xi_L = 5 \times 10^3/\mu\text{m}^2$ and $e_{RL} = 15 k_B T$ [1], we have $\gamma = 0.075\ k_B T/\text{nm}^2$. Considering an area-tunable nanoparticle with an effective radius of $a = 40$ nm interacting with a membrane with bending stiffness $\kappa_2 = 20 k_B T$ and tension $\sigma = 0.03$ mN/m [48], we have $\bar{\sigma} \approx 1.165$ and $\bar{\gamma} = 12$. As suggested in Fig. 6, such a nanoparticle with an initial reduced area $v = 0.6$ has a partial wrapping state and remains circulating before it reaches the target cell. As the nanoparticle reaches its target cell, an inflation of its reduced area to a value larger than 0.8 can be imposed to promote full wrapping followed by cell engulfment. This simple idea may be clinically useful as the remotely controlled drug delivery technology is under rapid development [49]. Elastic nanoparticles with or without area constraints can also be used to model or mimic many different types of nanoparticles such as hydrogel nanoparticles with high water content and pleomorphic viral particles appearing in different shapes in different situations.

A related but different phenomenon is the cell uptake of long one-dimensional (1D) nanomaterials via receptor-mediated endocytosis in which a near-perpendicular entry mode is preferred at a small normalized membrane tension $\bar{\sigma}$ but a near-parallel interaction mode prevails at sufficiently large $\bar{\sigma}$ [11]. In that case, endocytosis can usually be considered as a process limited by the diffusion of receptors in the cell membrane to the contact region [1,7]. Our previous study indicates that membrane wrapping regulated by two-dimensional diffusion of receptors is much faster than that regulated by one-dimensional receptor diffusion [1,11]. For 1D nanomaterials, the membrane wrapping of their curved tips should be governed by two-dimensional diffusion of receptors, while the wrapping of their cylindrical walls is regulated by one-dimensional diffusion of receptors. This means that the tip, rather than the lateral wall, of a 1D nanomaterial should be wrapped first. As long as the specific receptor-ligand interaction energy can overcome the deformation energy penalty induced by the tip wrapping, the subsequent interaction is governed by the two interaction modes controlled only by $\bar{\sigma} \equiv 2\sigma a^2/\kappa_2$ with a being the radius of cylindrical nanomaterials [11]. For three-dimensional short nanorods with two curved tips and a much smaller lateral wall, the difference between receptor diffusion near the tip and wall regions is not evident, whereas for short nanorods wrapped by membrane in two dimensions, as we focus in this study, the receptor diffusion is one-dimensional and has no difference between the tip and wall regions. In both cases, the specific receptor-ligand attractive interaction between short nanorods and cell membrane during the dynamic endocytosis can be approximated by adhesive interaction without the consideration of receptor diffusion as we did in the current study. Therefore, the initial wrapping of short nanorods would start at the relatively flat region of nanorods which appears to be a parallel configuration of the short nanorods with respect to the membrane. Such nanorods then reorient themselves perpendicular to the membrane during the late stage of wrapping regardless of the value of membrane tension as long as the adhesion energy is large enough. The orientational change from a parallel configuration to a perpendicular one relative to the membrane is characteristic of the mode of interaction between short rod-shaped nanoparticles and cell membrane.

V. CONCLUSIONS

We have performed a theoretical analysis related to the cellular uptake of elastic rod-shaped nanoparticles with a prescribed reduced area in two dimensions. Using sequential quadratic programming, we have calculated the system energy, determined the corresponding morphologies of nanoparticles and the cell membrane, and obtained the associated wrapping phase diagrams describing transition boundaries between different wrapping phases as well as the nanoparticle orientation phase diagram describing transition boundaries between different nanoparticle orientations. Compared to nanoparticles without any area constraint displaying symmetric morphology during the whole wrapping process, nanoparticles with a prescribed reduced area undergo a dramatic morphological change from a symmetric configuration in the early stage of wrapping to a symmetry breaking transition in the midstage, then to a symmetric configuration again in the late stage of wrapping. For nanoparticles without area constraints, stiffer particles always attain full wrapping more easily than softer particles [21]. The geometric constraint of a fixed reduced area complicates the wrapping phase diagram. In the cases of a relatively large normalized membrane tension $\bar{\sigma}$ and relatively small reduced area v, stiffer particles can attain full wrapping more easily than softer particles; in the cases of small $\bar{\sigma}$ and large v, the situations become complicated and no general conclusions exist. In the limiting case of rigid and relatively stiff nanoparticles, the particle shape evolves from a circle to a rod as the reduced area v decreases. We find that larger normalized adhesion energy $\bar{\gamma}$ is required to attain full wrapping for slender nanoparticles corresponding to smaller reduced area v. In other words, thinner and longer two-dimensional rigid or stiff nanoparticles require larger adhesion energy $\bar{\gamma}$ than thicker, shorter, and rounder ones for full wrapping.

This shape-dependent cellular uptake of short nanoparticles has also been observed in experiments [3–6]. Our results suggest that the particle elasticity and geometric restriction provide new design parameters to control cellular uptake and drug delivery processes. We also found that rigid and stiff rod-shaped nanoparticles align their long axes parallel to the membrane in the early stage of wrapping but suddenly reorient themselves with long axes perpendicular to the membrane and remain in this configuration in the late stage of wrapping. Such nanoparticle reorientation driven by the elastic deformation energy of the membrane is a generic mode of cell uptake of rod-shaped nanoparticles or any other relatively stiff short anisotropic nanoparticles. For soft nanoparticles, there exists a finite asymmetric morphological transition in the midstage of wrapping. The distinction in uptake between short rod-shaped nanoparticles and long one-dimensional nanomaterials is also discussed from the view of receptor-mediated endocytosis limited by diffusion of receptors.

The optimization method used here can be employed immediately in the study of interactions between multiple rigid [50–52] or soft particles in two dimensions, nanoparticle interaction with large cells [28,39], and elastocapillary interactions between droplets and soft structures such as lipid membranes [53] and elastic thin films [54]. This method can also serve as a foundation for future studies taking into account the deformation of a cytoskeleton network [55,56].

ACKNOWLEDGMENTS

The work reported has been supported by the National Science Foundation under INSPIRE: "Computational Design for the Safe Development of High-Aspect-Ratio Nanomaterials," Grant No. CBET-1344097, and one of its predecessor grants, Grant No. CMMI-1028530. This support is gratefully acknowledged.

[1] H. Gao, W. Shi, and L. B. Freund, Proc. Natl. Acad. Sci. USA **102**, 9469 (2005).
[2] S. Zhang, J. Li, G. Lykotrafitis, G. Bao, and S. Suresh, Adv. Mater. **21**, 419 (2009).
[3] B. D. Chithrani, A. A. Ghazani, and W. C. W. Chan, Nano Lett. **6**, 662 (2006).
[4] J. A. Champion and S. Mitragotri, Proc. Natl. Acad. Sci. USA **103**, 4930 (2006).
[5] L. Florez, C. Herrmann, J. M. Cramer, C. P. Hauser, K. Koynov, K. Landfester, D. Crespy, and V. Mailänder, Small **8**, 2222 (2012).
[6] J. W. Yoo and S. Mitragotri, Proc. Natl. Acad. Sci. USA **107**, 11205 (2010).
[7] X. Shi, A. von dem Bussche, R. H. Hurt, A. B. Kane, and H. Gao, Nat. Nanotechnol. **6**, 714 (2011).
[8] A. H. Bahrami, Soft Matter **9**, 8642 (2013).
[9] S. Dasgupta, T. Auth, and G. Gompper, Soft Matter **9**, 5473 (2013).
[10] S. Dasgupta, T. Auth, and G. Gompper, Nano Lett. **14**, 687 (2014).
[11] X. Yi, X. Shi, and H. Gao, Nano Lett. **14**, 1049 (2014).
[12] P. Decuzzi and M. Ferrari, Biophys. J. **94**, 3790 (2008).
[13] R. Vácha, F. J. Martinez-Veracoechea, and D. Frenkel, Nano Lett. **11**, 5391 (2011).
[14] K. Yang, B. Yuan, and Y.-Q. Ma, Nanoscale **5**, 7998 (2013).
[15] C. Huang, Y. Zhang, H. Yuan, H. Gao, and S. Zhang, Nano Lett. **13**, 4546 (2013).
[16] Y. Li, H. Yuan, A. von dem Bussche, M. Creighton, R. H. Hurt, A. B. Kane, and H. Gao, Proc. Natl. Acad. Sci. USA **110**, 12295 (2013).
[17] Y. Li, X. Li, Z. Li, and H. Gao, Nanoscale **4**, 3768 (2012).
[18] H.-M. Ding and Y.-Q. Ma, Biomater. **33**, 5798 (2012).
[19] H.-M. Ding and Y.-Q. Ma, Biomater. **34**, 8401 (2013).
[20] K. A. Beningo and Y. L. Wang, J. Cell Sci. **115**, 849 (2002).
[21] X. Yi, X. Shi, and H. Gao, Phys. Rev. Lett. **107**, 098101 (2011).
[22] B. Kaoui, G. Biros, and C. Misbah, Phys. Rev. Lett. **103**, 188101 (2009).
[23] H. Lei and G. E. Karniadakis, Biophys. J. **102**, 185 (2012).
[24] H. Lei and G. E. Karniadakis, Proc. Natl. Acad. Sci. USA **110**, 11326 (2013).
[25] M. Deserno, Phys. Rev. E **69**, 031903 (2004).
[26] W. T. Góźdź, J. Phys. Chem. B **109**, 21145 (2005).
[27] W. T. Góźdź, Langmuir **23**, 5665 (2007).
[28] J. Z. Y. Chen and S. Mkrtchyan, Phys. Rev. E **81**, 041906 (2010).
[29] B. J. Reynwar and M. Deserno, Soft Matter **7**, 8567 (2011).
[30] A. Šarić and A. Cacciuto, Phys. Rev. Lett. **109**, 188101 (2012).
[31] A. H. Bahrami, R. Lipowsky, and T. R. Weikl, Phys. Rev. Lett. **109**, 188102 (2012).
[32] P. B. Canham, J. Theor. Biol. **26**, 61 (1970).
[33] W. Helfrich, Z. Naturforsch. C **28**, 693 (1973).
[34] N. Ostrowsky and J. Peyraud, J. Chem. Phys. **77**, 2081 (1982).
[35] U. Seifert, Phys. Rev. A **43**, 6803 (1991).
[36] H.-G. Döbereiner, E. Evans, M. Kraus, U. Seifert, and M. Wortis, Phys. Rev. E **55**, 4458 (1997).
[37] J. Nocedal and S. J. Wright, *Numerical Optimization*, 2nd ed. (Springer, New York, 2006).
[38] See Supplemental Material at http://link.aps.org/supplemental/10.1103/PhysRevE.89.062712 for several supplemental figures from numerical calculations.
[39] Y. Zhao and Q. Du, Phys. Rev. E **84**, 011903 (2011).
[40] M. Raatz, R. Lipowsky, and T. R. Weikl, Soft Matter **10**, 3570 (2014).
[41] M. M. Müller, M. Deserno, and J. Guven, Phys. Rev. E **76**, 011921 (2007).
[42] S. A. Nowak and T. Chou, Phys. Rev. E **78**, 021908 (2008).
[43] R. Skalak, Science **164**, 717 (1969).
[44] Y. Hatano, M. Yoshida, F. Uno, S. Yoshida, N. Osafune, K. Ono, and M. Yamada, J. Electron Microsc. **50**, 113 (2001).
[45] D. K. Cureton, R. H. Massol, S. Saffarian, T. L. Kirchhausen, and S. P. J. Whelan, PLoS Pathog. **5**, e1000394 (2009).
[46] D. R. Beniac, P. L. Melito, S. L. deVarennes, S. L. Hiebert, M. J. Rabb, L. L. Lamboo, S. M. Jones, and T. F. Booth, PLoS One **7**, e29608 (2012).

[47] Y. Geng, P. Dalhaimer, S. Cai, R. Tsai, M. Tewari, T. Minko, and D. E. Discher, Nat. Nanotechnol. **2**, 249 (2007).
[48] C. E. Morris and U. Homann, J. Membr. Biol. **179**, 79 (2001).
[49] B. P. Timko *et al.*, Proc. Natl. Acad. Sci. USA **111**, 1349 (2014).
[50] T. R. Weikl, Eur. Phys. J. E **12**, 265 (2003).
[51] S. Mkrtchyan, C. Ing, and J. Z. Y. Chen, Phys. Rev. E **81**, 011904 (2010).
[52] P. Gosselin, H. Mohrbach, and M. M. Müller, Phys. Rev. E **83**, 051921 (2011).
[53] H. Kusumaatmaja and R. Lipowsky, Soft Matter **7**, 6914 (2011).
[54] A. Antkowiak, B. Audoly, C. Josserand, S. Neukirch, and M. Rivetti, Proc. Natl. Acad. Sci. USA **108**, 10400 (2011).
[55] P. Chen and V. B. Shenoy, Soft Matter **7**, 355 (2011).
[56] L. Li, X. Liu, Y. Zhou, and J. Wang, Biophys. J. **102**, 2230 (2012).